Int J Frac (2006) 141:227–246
DOI 10.1007/s10704-006-0075-6

ORIGINAL ARTICLE

On the effective constitutive properties of a thin adhesive layer loaded in peel

Tobias Andersson · Anders Biel

Received: 12 October 2005 / Accepted: 11 April 2006

Abstract An experimental method to determine the complete stress-elongation relation for a structural adhesive loaded in peel is presented. Experiments are performed on the double cantilever beam specimen, which facilitates a more stable experimental set-up as compared with conventional methods like the butt-joint test. The method is based on the concept of equilibrium of the energetic forces acting on the specimen. Two sources of energetic forces are identified: the start of the adhesive layer and the positions of the two acting loads. By use of the concept of equilibrium of energetic forces, it is possible to measure the energy release rate of the adhesive layer instantaneously during an experiment. The complete stress-elongation relation is found to be the derivative of the energy release rate with respect to the elongation of the adhesive layer at its start. By this procedure, an effective property of the adhesive layer is measured. That is, the fields are assumed to be constant through the thickness of the layer and only vary along the layer. To investigate the validity of this approach, experiments are performed on five different groups of specimens with different dimensions. This leads to large variations in the length of the damage zone at the start of the adhesive layer. Four of the experimental groups are used to determine the stress-elongation relation. This is found to be independent of the geometry. For the remaining experimental group, the adherends deform plastically and simulations are performed with the stress-elongation relation determined from the four elastic groups. It is found that the relation cannot be used to accurately predict the behaviour of the experiments where the adherends deform plastically. This indicates that the stress-elongation relation has limited applicability.

Keywords Stress-elongation relation · Adhesive layer · Experimental method · Energetic force · J-integral · Damage zone · Anticlastic deformation

T. Andersson (✉) · A. Biel
Department of Engineering Science, University of Skövde P.O. Box 408, SE-541 28 Skövde, Sweden
e-mail: tobias.andersson@his.se

1 Introduction

In recent years, the automobile industry has shown an increasing interest in adhesive joining. The major driving force behind this is the need to lower the weight of the car in order to reduce fuel consumption and emissions. With the conventional spot-welding procedure, which dominates the automobile industry today, rather low-strength steel sheet metal can be handled successfully. In order to be able to use advanced alloy steels, light metals and composites, adhesive joining appears

to be one of the most promising joining technologies. With adhesive joints, a wider choice of materials can be considered in the design process. For example, by using structural foams between frame sections instead of steel reinforcements the weight of the car can be substantially reduced. This will also lead to improved crash performance and to a higher torsional stiffness, which are desirable properties. However, to guarantee the reliability of the car, the adhesive between the foam and the steel section must be strong enough to hold during a crash. There is therefore a need for good material models and accurate data to be used in numerical simulations during the design process. However, these data are not easily obtained.

An engineering adhesive is a highly non-homogeneous material. The adhesive often consists of different types of filler particles with different functions. Silicate particles are often used to increase the stiffness and toughness; Rubber particles are used to increase the flexibility and the toughness. As a consequence of these particles, the deformation and fracture process of the adhesive layer become very complicated. Salomonsson and Andersson (2005) have performed a scanning electron microscope (SEM) study of the present adhesive, DOW BETAMATE XW-1044. This study reveals that the adhesive consists of an epoxy/thermoplastic blend, which acts as a matrix in a composite, and mineral regions, *cf.* Fig. 1a. Here, the white regions are the mineral. These contain small grains of mineral with a size of 4–10 μm. A peel test has been performed in the SEM to study the fracture process. This process is found to be rather complicated (Fig. 1b). From this it is observed that micro-cracks initiate in the mineral regions; preferable in the larger regions in-between the grains. Later, the micro-cracks in the mineral regions coalesce with other mineral regions and form macroscopic cracks that unload the regions above and below the cracks. Thus, the strain is localised both to different regions along the layer and also to different regions through the thickness of the layer. Since the two constituents in the layer have different stiffness and fracture properties the stress along the layer fluctuates.

A substantial amount of early work on the strength of adhesive joints is based on linear-elastic fracture mechanics (LEFM) and several standards are based on this concept, for example, the ASTM D3433 (1999) and the British Standard, BS7991:2001 (2001). By using LEFM, the actual fracture process taking place in the adhesive is disregarded and it is assumed that the damage zone is much smaller than other relevant dimensions, e.g. the layer thickness. Ideally, the length of the damage zone is considered to be zero in LEFM. In order to compensate for the actual dimensions of the damage zone, some of the standards introduce methods for correction. The correction terms are determined from the experimental results. Depending on the choice of evaluation method, the results from the standards differ when applied to a tough engineering adhesive, (Biel 2005). For example, the use of ASTM D3433 typically underestimates the fracture energy. For most of the methods the error decreases with an increasing crack length although the suggested crack length in ASTM D3433 appears to be too small to yield a good estimate of the fracture energy.

The length of the damage zone depends on several factors, for example, the ductility of the adhesive and the geometry of the specimen, for example, Cavalli and Thouless (2001). In practice the damage zone can be very large. As shown here, the length of the damage zone is of the same order of magnitude as the height of the adherends for an engineering adhesive loaded in peel. In shear, the length is found to be substantially larger than the height of the adherends (Leffler et al. 2005). Thus, LEFM appears unfit to predict the strength of many engineering adhesive joints.

For large scale structural analyses it is preferable that the model of the behaviour of the adhesive joint is simple in order to reduce the computational time. There is therefore a need for simplifications. In a structural analysis the behaviour of the adhesive layer is preferable modelled with interface elements in which the tractions from the adhesive layer are assumed to be determined from the separation of the layer (Yang et al. 1999; Su et al. 2004). Therefore, in this study we employ what we refer to as the adhesive layer theory. In the case of a soft and thin *elastic* layer, this method is motivated by an asymptotic expansion analysis by Klarbring (1991) who shows that the two deformation modes indicated in Fig. 3 dominates. In this theory, the stresses and strains are averaged over

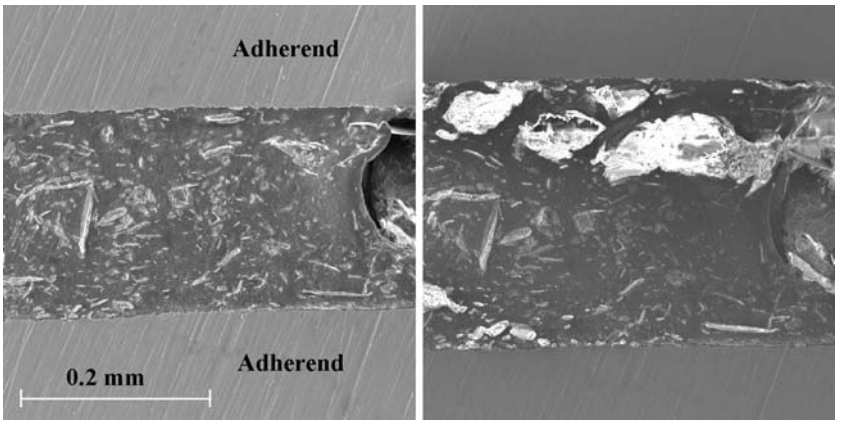

Fig. 1 Scanning electron microscope (*SEM*) images of the adhesive layer. (**a**) Undeformed state; (**b**) deformed state

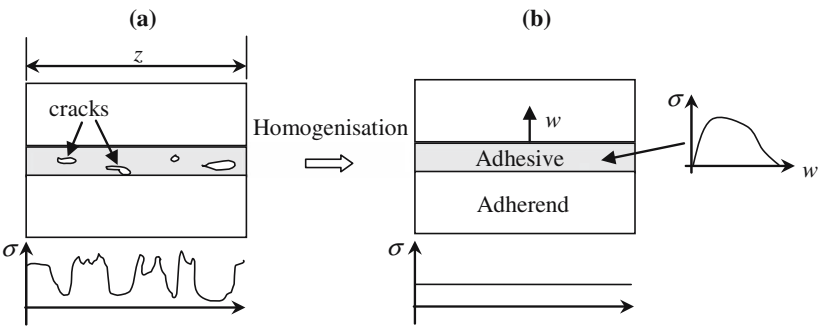

Fig. 2 Schematic illustration of the adhesive layer theory

the thickness of the adhesive layer. Therefore, the layer can be regarded as a layer of distributed nonlinear springs.

Using the adhesive layer theory, we do not explicitly model the geometrical features of the fracture process. However, in the constitutive modelling we incorporate the fracture process of the adhesive (Fig. 2a, b). Even though the microstructure of the adhesive is complex (Fig. 1b) the adhesive is considered homogenous. This is obviously not the case for the present adhesive layer since the two constituents have substantially different properties. However the mineral regions are located randomly and the through-thickness properties for different positions along the layer should be practically the same. The stresses along the layer may fluctuate, especially when larger cracks start to appear in the layer, (Fig. 2a). However, over a certain length, z, the stresses can be averaged out and form a homogenized smooth macroscopic stress (Fig. 2b). Plasticity and various damage mechanisms that occur in the adhesive layer are all inherent features of the traction-separation relation. Thus, the traction-separation relation is considered to be an effective property.

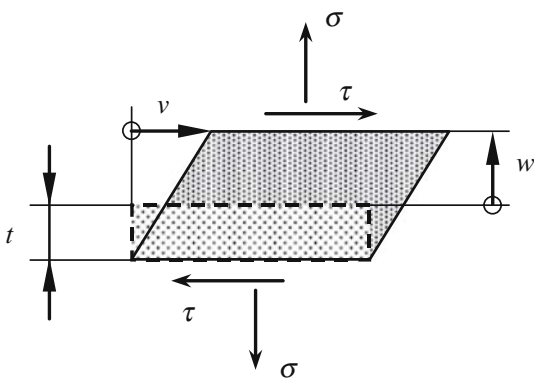

Fig. 3 Deformation modes of the adhesive layer with thickness t: peel, w, and shear, v. Conjugated stress components are σ and τ

In the general case, the layer is described with the peel (tension) stress, σ, the shear stress, τ, the elongation, w, and the shear deformation, v, as basic variables (Fig. 3). Thus, in the elastic case the adhesive layer can be described by the stress-elongation relations $\sigma(w, v)$ and $\tau(w, v)$. In this paper we only consider peel (tension) loading.

In a parallel project, the end notch flexure specimen (ENF) is used to determine the $\tau(\nu)$ relation experimentally for the same adhesive layer. Experimental results based on the ENF-specimen are given by Alfredsson et al. (2003) and Leffler et al. (2006). The mixed-mode behaviour is studied by Högberg and Stigh (2006).

To determine the $\sigma(w)$ relation, an inverse method is utilized (Olsson and Stigh 1989). This is due to the fact that many adhesives show softening and as a consequence, the $\sigma(w)$ relation is more easily obtained with a specimen that has a non-homogenous state of stress. Andersson and Stigh (2004) have performed a series of experiments on the double cantilever beam specimen (DCB) (Fig. 4). This type of specimen facilitates a more stable experimental set-up as compared to specimens with a homogenous state of stress, for example, the butt-joint. To understand this, consider a failure process where multiple microscopic cracks develop in the adhesive layer. In a butt-joint, these cracks will develop uniformly in the adhesive layer. Thus, when the cracks reach their critical state, all cracks will fail simultaneously and the joint will fail in a catastrophic manner. In a DCB-specimen, microscopic cracks first develop at the loaded side of the adhesive layer and form a damage zone. This zone contains larger microcracks at the loaded side and gradually fewer and smaller cracks as we move away from the loaded side. Thus, when the cracks at the loaded side of the adhesive layer reach their critical size and a macroscopic crack develops, undamaged material remains to hold the load. Thus, the DCB-specimen is more stable. For the DCB-specimen the relation between the peel stress and the elongation is given by

$$\sigma(w) = \frac{dJ}{dw} = \frac{2}{b}\frac{d(F\theta)}{dw} \tag{1}$$

where J is the path independent J-integral (Rice 1968) and is identified as the "applied" energetic force, $F\theta/b$ due to the acting load F (Stigh and Andersson 2000). The factor 2 in Eq. 1 is due to the fact that two forces load the specimen. Here, θ is the rotation of the loading point and b is the out-of-plane width of the specimen. The elongation of the adhesive layer at the start of the layer is denoted w. The energetic "load" on the adhesive layer is identified as $\int \sigma(w)dw$. With this interpretation of the terms in Eq. 1, this equation can be identified as a differentiated equilibrium equation, i.e. equilibrium of energetic forces. An experiment thus consists of a simultaneous measurement of the applied energetic force per unit width $J = 2F\theta/b$ and the elongation w.

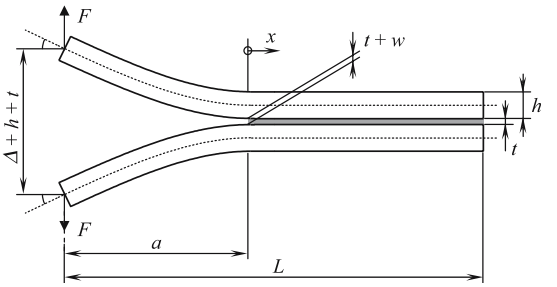

Fig. 4 Double cantilever beam (*DCB*)-specimen

As evident, a drawback with the work performed by Andersson and Stigh (2004) is that the interferometric method used in that paper to measure w made it impossible to obtain the last part of the $\sigma(w)$ relation. Moreover, it is not possible to identify the moment at which a macroscopic crack starts to propagate. Therefore, a microscope is used in the present study to record the fracture process at the start of the adhesive layer during the experiment. With the microscope, it is also possible to make an estimate of the length of the damage zone in the adhesive layer.

A similar approach to measure the $\sigma(w)$ relation is employed by Sørensen (2002). However, instead of applying forces at the end of the DCB specimen, the specimen is loaded with applied bending moments, M, at the free end. The main difference is the measurement of the applied energetic force per unit width which, in this case, is given by $J = 12M^2/b^2h^3E$ for plane stress. Thus, it is only necessary to measure the applied moments and the elongation during an experiment. However, the material and geometrical properties, E, b and h, must be measured carefully. By performing simulations and experiments on a different type of geometry, Sørensen is able to predict the experiments using the $\sigma(w)$ relation obtained from experiments with the DCB-geometry. As compared with the present work, Sørensen studies a polyurethane adhesive, which is expected to possess

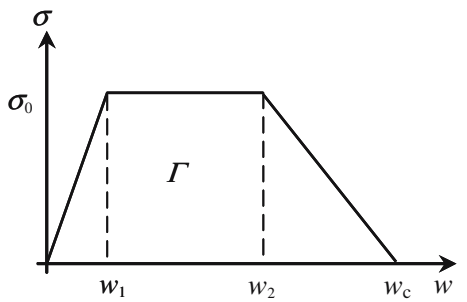

Fig. 5 $\sigma(w)$ relation of the Embedded-process-zone (EPZ) model

fundamentally different properties than the epoxy adhesive studied here.

A different strategy is applied by Yang et al. (1999). Similarly as Sørensen (2002), they perform experiments on the DCB specimen, in this case loaded with a wedge moving along the two free interfaces of the specimen. However, in their case the adherends deform with extensive plastic deformations. An embedded-process-zone (EPZ) model, (Fig 5) is used to characterise the σ–w relation of the adhesive layer and the parameters in the EPZ-model are determined by calibrating simulations to experimental results. Thus, contrary to the two methods above, it is not possible to determine the shape of the of σ–w relation; it is assumed a priori. However, in these experiments the adherends are allowed to deform plastically and the damage zone in front of the start of the adhesive layer becomes considerably shorter in comparison to cases where the adherends deform elastically. An important issue is whether this affects the $\sigma(w)$ relation since, for a specific "applied" energetic force J, specimens with different heights of the adherends give various lengths of the damage zone and consequently a different state of stress in the damage zone.

Cavalli and Thouless (2001) have compared the toughness of an adhesive layer obtained from experiments performed with elastically and plastically deforming adherends. They found that the fracture toughness differ significantly with the behaviour of the adherends. They argue that with elastically deforming adherends, the constraint is increased and voids nucleate and grow ahead of the crack tip before a macroscopic crack develops. With plastically deforming adherends, they found the macroscopic crack to propagate continuously without any significant damage growth in front of the crack tip. Thus, with elastically deforming adherends, the fracture energy is significantly larger than with plastically deforming adherends. As a consequence, the toughness is not a property associated with the adhesive layer. These results indicate that the adhesive layer theory has a limited applicability. Since the size of the area under the σ–w curve equals the fracture energy, and this energy apparently varies with the constraints of the adherends, also the σ–w curve is dependent of the behaviour of the adherends. Thus, it is important to determine the conditions for the validity of the adhesive layer theory.

The aim of the present paper is to extend the work presented in Andersson and Stigh (2004). In that paper only minor variations of the specimen geometry are studied. Here, we attempt to test the applicability of the method by performing experiments on five groups of specimens with different dimensions. For four of these experimental groups we determine the $\sigma(w)$ relation using Eq. 1 and investigate if the relation is dependent of the tested geometry. For the remaining group, we perform experiments where the adherends deform with extensive plastic deformation before a crack propagates in the adhesive layer. By performing simulations using the $\sigma(w)$ relation obtained from the experiments where the adherends deform elastically, we investigate if the relation can be used to predict the behaviour of the experiments with plastically deforming adherends.

2 Theory

In this study we merely present the main features of the derivation of Eq. 1. Detailed derivations are given by Olsson and Stigh (1989), Stigh and Andersson (2000) and Andersson and Stigh (2004). The underlying theory behind Eq. 1 is based on the concept of equilibrium of energetic forces as introduced by Eshelby (1951). The energetic force for an object is given by

$$\mathbf{J} = -\frac{\partial \prod}{\partial \xi} \tag{2}$$

where Π is the potential energy and ξ denotes the position of the object. Thus, **J** is the "force on the object" associated with a variation of its position; sometimes denoted the "material" or "configurational" force. It should be noted that the energetic force is not a force in the conventional sense. The notion of an *object* is central in this context.[1] By an object we mean all features of a body and its loading that alters the potential energy of the body, when they are moved to a different location. For instance, if the motion of a boundary of a body alters the potential energy, then the boundary is an object and an energetic force is associated with it. It should be emphasized that the movement of the object should be interpreted as virtual.

For a homogenous elastic material in small deformation, the x-component of **J**, J_x, is the path-independent J-integral,

$$J_x = \int_S \left(W n_x - \mathbf{T} \cdot \frac{\partial \mathbf{u}}{\partial x} \right) dS \tag{3}$$

where S is a curve surrounding the object, W is the strain energy density, n_x is the x-component of the outward normal to the path S, **T** is the traction vector defined by $T_i = \sigma_{ij} n_j$, and **u** is the displacement vector. With prescribed forces, F, the potential energy Π of the DCB specimen is determined by the position of the acting forces (F) and the position of the start of the adhesive layer. Thus, the energetic forces are associated with the positions of the acting loads (F) and the start of the adhesive layer (a) (Fig. 4). The far end of the specimen is not deformed if the specimen is long enough and Π does not change with its position. Thus, no energetic force is associated to its position. The details of the derivation of the energetic forces are given by Stigh and Andersson (2000). The result is

$$J_F = -\frac{F\theta}{b}, \quad J_{\text{adhesive}} = \int_0^w \sigma\left(\tilde{w}\right) \mathrm{d}\tilde{w}. \tag{4a, b}$$

Equilibrium of the acting energetic forces yields

$$\int_0^w \sigma\left(\tilde{w}\right) \mathrm{d}\tilde{w} = \frac{2F\theta}{b} \tag{5}$$

The factor 2 is due to the fact that two forces (F) act on the specimen. Differentiating Eq. 5 yields Eq. 1.

A major benefit with the present method is that both the bending moment and the transverse shear force are accounted for in the derivation of the applied energetic force J_F. Thus, irrespective of whether the loading is moment or force dominated, the method still applies. This makes the approach insensitive to the type of loading.

In an experiment the force, F, the rotation of the loading point, θ, and the elongation, w, are to be measured continuously. It should be stressed that these quantities are measured *before* the crack starts to propagate. In addition, it is not necessary to know the exact location of the crack tip since the crack length does not enter Eq. 1 explicitly. This is one of the merits with this method since it is often difficult to measure the position of a running crack tip.

The $\sigma(w)$ relation is found by either making a direct differentiation of the measured data or by using a curve fitting procedure and then differentiating the fitted curve. In this paper the latter method is adopted.

A critical requirement for the validity of the method is that a unique stress-deformation relation is associated with the adhesive layer. Thus, if the adhesive layer is unloaded from a non-elastically deformed state, the theory breaks down, [Eq. 3]. This requirement is easily checked by use of the finite element method (Andersson and Stigh 2004).

3 Experimental set-up for property determination

3.1 Experimental set-up

The tensile test machine is shown in Fig. 6. It consists of two yokes each moving in opposite direction. The yokes hold two horizontal forks in which one is connected to a force transducer. The grip, which holds the test specimen, is connected to the fork by two axes. For the axes to rotate freely four bearings are utilized; two bearings mounted to the fork and two mounted on the grip. The measurement system consists of a force transducer, a shaft encoder and two linear variable displacement

[1] Eshelby prefered the word "singularity".

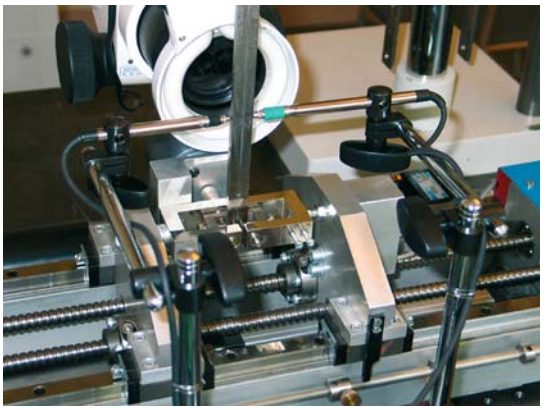

Fig. 6 Tensile test machine

transducers (LVDT). The shaft encoder is used to measure the rotation, θ, at the loading point and the LVDT's are used to measure the elongation, w. The LVDT's are placed at opposite sides of the adherends. The transverse deformation of the adherends is small in comparison with the elongation of the layer itself. Thus, the LVDT's measure the elongation of the layer (Fig. 4).

3.2 Design of specimens for property determination

A feature that may have a large influence on the $\sigma(w)$ relation is the size of the damage zone developing at the start of the adhesive layer during loading. For the DCB specimen, it can be demonstrated that the height of the adherends have a large effect on the size of the damage zone; stiff adherends lead to large damage zones. Thus, in the present study the main emphasis is set to alter the height of the adherends.

Numerical simulations are used to determine the expected length of the damage zone, d. The simulations are performed using the commercial finite element code ABAQUS (version 5.8). The adherends are modelled with beam elements (B21) and the adhesive layer is modelled with spring elements (SPRING1). The length l_e of the beam elements is 0.1 mm in all the simulations in order to capture the gradients in the stress-field. The force-displacement relation for the spring elements is based on the $\sigma(w)$ relation in Fig. 5. This model is very similar in shape to the experimental $\sigma(w)$ curves in Andersson and Stigh (2004). The model is used by Tvergaard and Hutchinson (1992) to describe the fracture process in an elastic-plastic solid. In the following we will denote this the EPZ model. The parameters are adapted to the experimental results of Andersson and Stigh (2004). In reasonably agreement with the experiments the fracture energy is set to $J_c = 800\,\mathrm{J/m^2}$ and the parameters for the displacement are set to $w_1 = 3\,\mu\mathrm{m}$, $w_2 = 20\,\mu\mathrm{m}$ and $w_c = 60\,\mu\mathrm{m}$. With these values the maximum stress becomes $\sigma_0 = 2J_c/(w_c + w_2 - w_1) = 21\,\mathrm{MPa}$. The length of the damage zone is here defined as the distance between the start of the adhesive layer, $x = 0$, and the position along the layer at which $w = w_1$. The maximum length of the damage zone is denoted d_s (where the subscript s indicates simulation). In a simulation this is attained when the crack is just about to propagate. Generally, this occurs somewhat after the applied force has started to decrease. Four different groups of specimens are designed to achieve a large variation of the size of the damage zone. The nominal dimensions of the specimens and the approximate lengths of the damage zone are given in Table 1.

It is also possible to evaluate the size of the damage zone approximately using a closed form solution by Stigh (1988). Here, the stress-elongation relation is described by a saw-tooth shaped curve. The saw-tooth is described by the fracture energy J_c, the elongation w_0 at which the maximum stress occurs and the maximum elongation, w_c. With $J_c = 800\,\mathrm{J/m^2}$, $w_0 = 3\,\mu\mathrm{m}$ and $w_c = 60\,\mu\mathrm{m}$ the damage zone length d_a (where the subscript a indicates analytical) is calculated. The values of the length of the damage zone d_a are also given in Table 1.

It is noted that the EPZ and the saw-tooth models give similar lengths of the damage zone. As expected, the stiffer adherends give a larger damage zone. Generally, the damage zone is many times larger than the thickness of the adhesive layer. The relation between the length of the damage zone and the height of the adherends is used in ASTM D3433 as a criterion for the validity. To be a valid experiment this relation should be small. In this study d_a and d_s are both longer than h in all groups.

By varying the dimensions of the specimen the length of the damage zone is varied with a factor 3 between the experimental groups. It should be

Table 1 Dimensions and length of damage zone

	Group 1	Group 2	Group 3	Group 4
$b \times h \times L$ (mm)	$5 \times 4.5 \times 150$	$5 \times 10.6 \times 200$	$5 \times 16.6 \times 400$	$5 \times 20.7 \times 400$
a (mm)	50	120	200	250
d_a (mm)	8	15	21	24
d_s (mm)	7	14	18	23

noted that the length L is not a critical value as long as the specimen is long enough to be considered semi-infinite. This is the case for all groups.

The adherends are made of steel with Young's modulus, $E = 206$ GPa and a yield strength, $\sigma_Y \geq 500$ MPa. The high yield strength prevents the adherends to deform plastically. Note that no material data enters Eq. 1 explicitly.

Before applying the adhesive, the surfaces of the adherends are cleaned with *n*-Heptane and subsequently washed with acetone. After cleaning, the adhesive is smeared out on one of the adherends and the adherends are pressed together. In this process, Teflon-inserts with a thickness of 0.2 mm are used to achieve the correct adhesive layer thickness. The adhesive is then cured at 180°C for about 30 min according to the specification of the manufacturer. The oven is then turned off and the specimens are allowed to cool slowly to room temperature, thus reducing the residual stresses. All the specimens of each Group are cured at the same time. By this process, we minimize possible effects of variations in the manufacturing process.

All the specimens, except for the adherends in Group 2 are cut to the correct dimensions before gluing. The adherends in Group 2 are manufactured by pressing two steel plates together in a fixture. The specimens are then cut to their specific dimensions after the curing and cooling process.

4 Experimental results—property determination

All the experiments are performed with a prescribed velocity of $\dot{\Delta} \approx 0.01$ mm/s. As a result, the velocity at the start of the layer $\dot{w}|_{x=0}$ varies between 0.15 and 0.3 μm/s for all the groups. Rate effects have been studied separately. That study reveals that the adhesive is rate dependent, however for the present variation of 0.15–0.3 μm/s the rate effect is small and do not influences the results (Biel 2005).

4.1 Determination of the $\sigma(w)$ curves

The experimental $J(w)$ curves are shown in Fig. 7. The curves appear smooth and regular indicating that the experiments are well performed.

Figure 7a shows that the $J(w)$ curves of Group 1 agree well for all w. In the initial part of the curves, J increases almost parabolically. The curves continue with a nearly linear part up to $w \approx 0.03$ mm with a corresponding value of J of about 500 J/m^2. At this point the slope of the curves decreases and J reaches, asymptotically, a value of about 650 J/m^2. Visual inspection of the fracture surfaces of the specimens in Group 1 indicates a rough surface along the entire fracture surface.

Figure 7b shows the $J(w)$ curves from Group 2. These curves show a similar behaviour as for Group 1. However, the curves indicate a larger scatter in J between the mutual experiments. In these experiments, the curves have a longer linear part in comparison to the curves of Group 1. In addition, the curves reach asymptotically the value $J \approx 700$ J/m^2, which is slightly larger than for Group 1. For small w, two of the curves of Group 2 deviate from the other. This is due to problems in the measurement of w for small values. However, this part is of minor importance since it only affects the initial slope of the $\sigma(w)$ curve. The dotted curve in Group 2 has a lower initial slope indicating a weaker bond of the layer. Inspection of the fracture surface of this specimen indicates interfacial fracture. This is probably caused by inherent damage in the adhesive layer or by micro-cracks that initiate prematurely at the interface and give rise to an increased crack length. This experiment is regarded as a failure and is not considered in the sequel. Note that the maximum value of J is almost

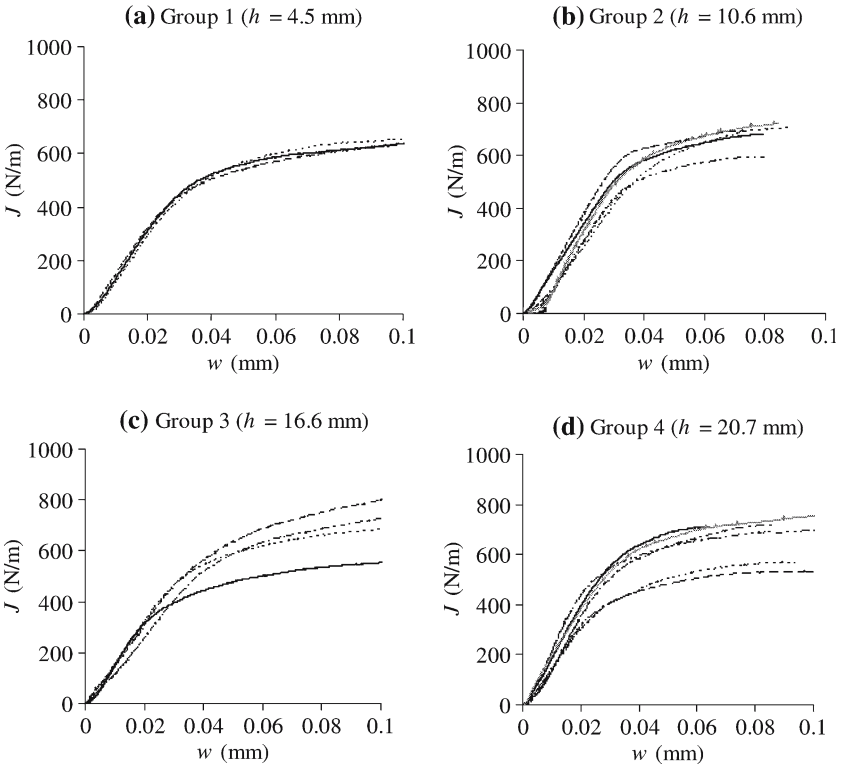

Fig. 7 Experimental $J(w)$ curve

the same for this experiment as compared to the other.

Figures 7c and d show the $J(w)$ curves from Groups 3 and 4. The shape of these curves is similar to Group 1. There is a notably larger scatter of the curves of Groups 3 and 4, especially for the last part. One experiment of Group 3 substantially deviates from the other (Fig. 7c). In this test the fracture surface shows evidence of cavities at the start of the layer. These cavities are small and do not have any influence on the load carrying area. As a consequence they do not influence the stiffness or the maximum stress. However, they may introduce stress concentrations which are likely to initiate small cracks at a high stress level; probably at the maximum stress. During further loading the cracks propagate and the layer looses its load bearing capacity. This probably explains the low value of J. In Group 4, two curves deviate. One of the specimens indicates cavities at the start of the layer and the other has a considerably smoother fracture surface than the others. The smooth fracture surface corresponds to smaller fracture energy.

The $\sigma(w)$ relation is derived by first fitting a Prony-series to the experimental $J(w)$ data. The series is given by

$$\frac{J(w)}{J_{\max}} = \sum_{i=1}^{n} A_i \exp\left(-\frac{nw}{iw_{\max}}\right) \tag{6}$$

where the constant A_i is determined by means of the least square method. Here, $J_{\max}$ is the maximum value of J found in the experiments and $w_{\max}$ is the corresponding value of w. The number of terms, n, varies from 10 to 15; the number is chosen based on visual inspection of the adopted and the experimental curves. The finally chosen number depends on the experimental group. The resulting $J(w)$ curves are then differentiated according to Eq. 1. The results are shown in Fig. 8. The experiments show a maximal peel stress σ_0 that varies between 17 and 27 MPa. The $\sigma(w)$ curves agree well within, and fairly well between, the experimental groups. However, slight variations exist in each group, especially in Groups 2 and 4, which show larger scatter as compared with Groups 1 and 3. In addition, the $\sigma(w)$ curves are in good

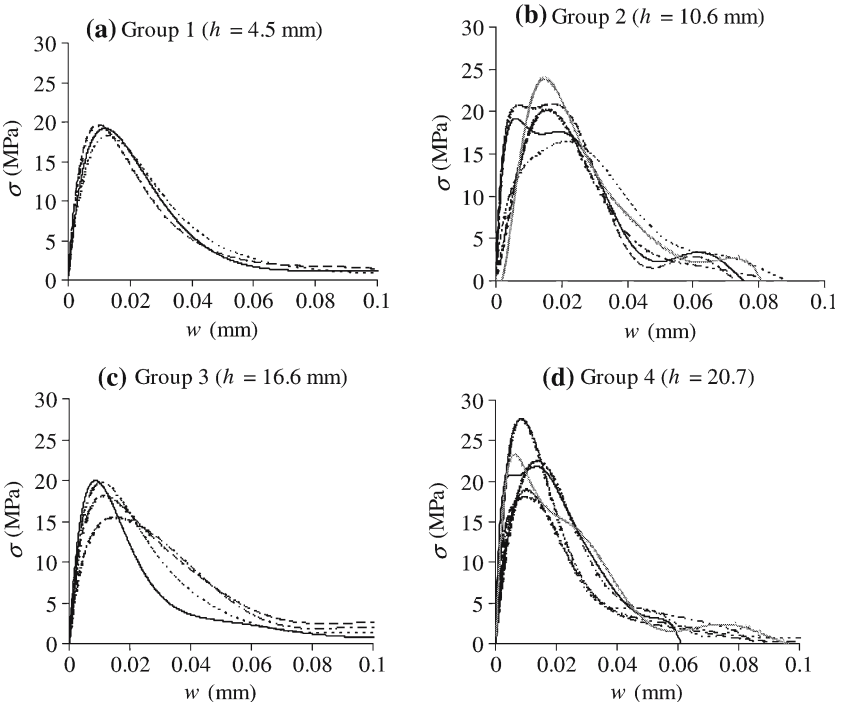

Fig. 8 Experimental $\sigma(w)$ relations

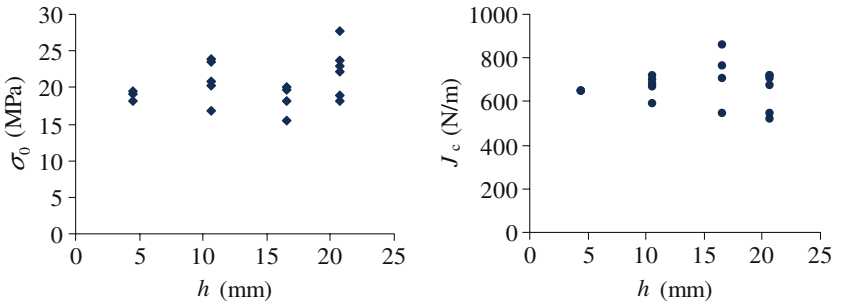

Fig. 9 Experimental results from the four groups. (*Left*) Maximum stress σ_0. (*Right*) Fracture energy J_c

agreement with the experimental results of Andersson and Stigh (2004).

A number of $\sigma(w)$ curves have a long tail where the stress level is negligible in comparison with the maximum stress and the contribution to J is small. Therefore this part of the curve contributes only marginally to the strength of the adhesive joint. In order to obtain a useful constitutive relation, the curves are cut-off at $\sigma = 0.05\sigma_0$ which yields a corresponding value, $w = w_c$. The fracture energy J_c is taken as the area under the $\sigma(w)$ curve from $w = 0$ to $w = w_c$.

A summary of the experimental results of σ_0 and J_c is given in Fig. 9. The average values of the maximum stress and the fracture energy correspond well between the experimental groups. Thus, no significant difference is observed between the different specimen designs. If we compile data from all four groups, the mean value and the standard deviation for the maximum stress are found to be 20.5 and 3 MPa, respectively. Moreover, the mean value and the standard deviation for the fracture energy are 680 and 82 J/m^2, respectively.

In order to study the deformation process and the initiation and evolution of cracks during the experiments, the start of the adhesive layer is recorded with a microscope. Figure 10 shows the start of the adhesive layer at six different stages of deformation. The corresponding points in the $\sigma(w)$ curve are depicted in Fig. 11.

Figure 10a shows the undeformed state with the Teflon film visible in the lower part of the image.

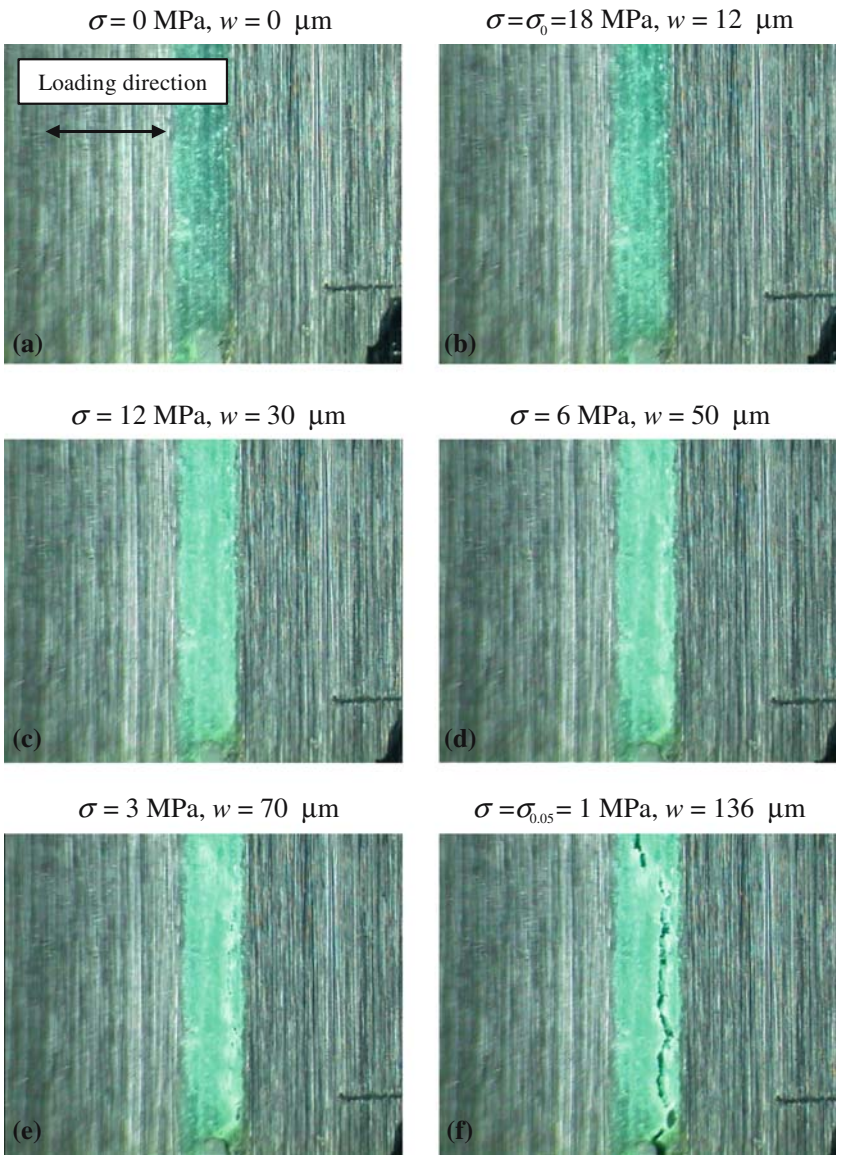

Fig. 10 Deformation of the adhesive layer at different values of the elongation w. Corresponding *triangular markers* are shown in Fig. 11

The thickness of the adhesive layer is 0.2 mm and the visible length of the layer is approximately 1 mm. In Fig. 10b, the maximum stress is reached and stress whitening becomes apparent. At this magnification the stress whitening seems evenly distributed through the adhesive layer. However, at a larger magnification one actually observes narrow bands of localized damage that orientate parallel to the layer in a zigzag fashion (Salomonsson and Andersson 2005). Figure 10c shows the crack-tip region at $w = 30\,\mu$m. At this state, the stress whitening has increased which indicates an enhancement of damage through the entire layer.

At further loading, a localization of stress whitening near one of the interfaces is observed (Fig. 10d). This is a trend observed in almost all the experiments. In addition, at this stage, the overall stress whitening has reached its maximum. In Fig. 10e, the initiation of a macroscopic crack is visible. The overall whitening is somewhat less in comparison with the maximum achieved during the experiment. This indicates that this region of the adhesive layer unloads when a larger crack is

formed. In Fig. 10f, a crack is almost fully developed, however, small ligaments still bond the adhesive. These ligaments probably cause the long tail observed in most of the $\sigma(w)$ curves (Fig. 8).

Different levels of damage growth occur along the layer due to the inhomogeneous material. Thus, micro-cracks develop at different positions along the layer and, as a consequence, the stress distribution along the layer is not continuous and smooth, but varies. Despite the complex deformation process, the $\sigma(w)$ curves in Fig. 8 are fairly consistent. Thus, with a length of the damage zone varying from about 7 to about 23 mm, the same $\sigma(w)$ relation can be used.

4.2 Evaluation of the $F(\Delta)$ and $J(\Delta)$ curves

According to the adhesive layer theory, J should be constant during crack propagation. Any deviation from the constant value indicates that the layer behaves differently along the layer. The experimental $J(\Delta)$ curves in Fig. 12 show that the adhesive layer behaves differently along the layer. This can be observed in Group 1 where J reaches a maximum value of about 750 J/m^2 at $\Delta \approx 2$ mm. In the subsequent crack propagation, J varies with Δ, which indicates that the fracture energy along the adhesive layer varies. This is probably due to different fracture processes along the layer, which may be due to the inhomogeneous material. However, J varies only slightly during crack propagation. The mean value of J during crack propagation may be taken as the critical value, J_c. As explained earlier, another method is used to extract the fracture energy in the present paper. From Fig. 12, it is also observed that the maximum value of J varies between 700 and 800 J/m^2 for nearly all the experiments.

As apparent from Fig. 10, no sharp crack tip develops during the experiments. Rather the crack tip is preceded by a large damage zone where a number of micro-cracks develop. This observation, together with the small variation of J_c (Fig. 12) during crack propagation, indicates that the lack of a sharp initial crack tip in the present approach gives a negligible effect.

Load versus load-point deflection, that is, the $F(\Delta)$ graphs are shown in Fig. 13. The initial increasing part of the curves appears fairly consistent for each group indicating that the experiments have been well performed. It is noted that Groups 3 and 4 provide a larger scatter of the maximum force as compared with Groups 1 and 2.

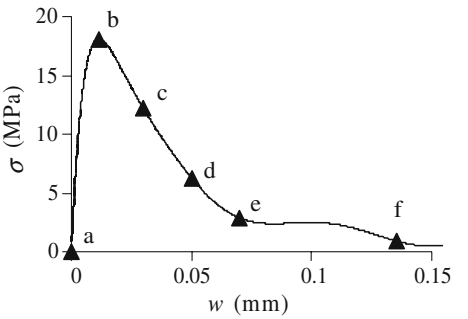

Fig. 11 Points on the $\sigma(w)$ curve corresponding to the images in Fig. 10

5 Plastically deforming specimens

In this section we investigate if the $\sigma(w)$ relation determined by the method described earlier can be used to predict the experimental behaviour if the adherends deform plastically. As mentioned, plastically deforming adherends leads to a substantially shorter damage zone. A DCB specimen is designed to give substantial plasticity before the adhesive breaks and the crack start to propagate. In the following we will designate these specimens as Group 5.

5.1 Design of the plastically deforming specimens

When designing the specimens, the main emphasis is put on achieving a significant amount of plastic deformation of the adherends before a macroscopic crack starts to propagate in the adhesive layer. This is partly accomplished by choosing a small value of the height h of the specimen and in part by using mild steel.

The design of the specimens is conducted in the same way as in the elastic case, that is, the adherends are modelled with beam elements and the adhesive layer with spring elements. The $\sigma(w)$ relation for the spring elements is described by a curve that has been adapted to a typical experimental

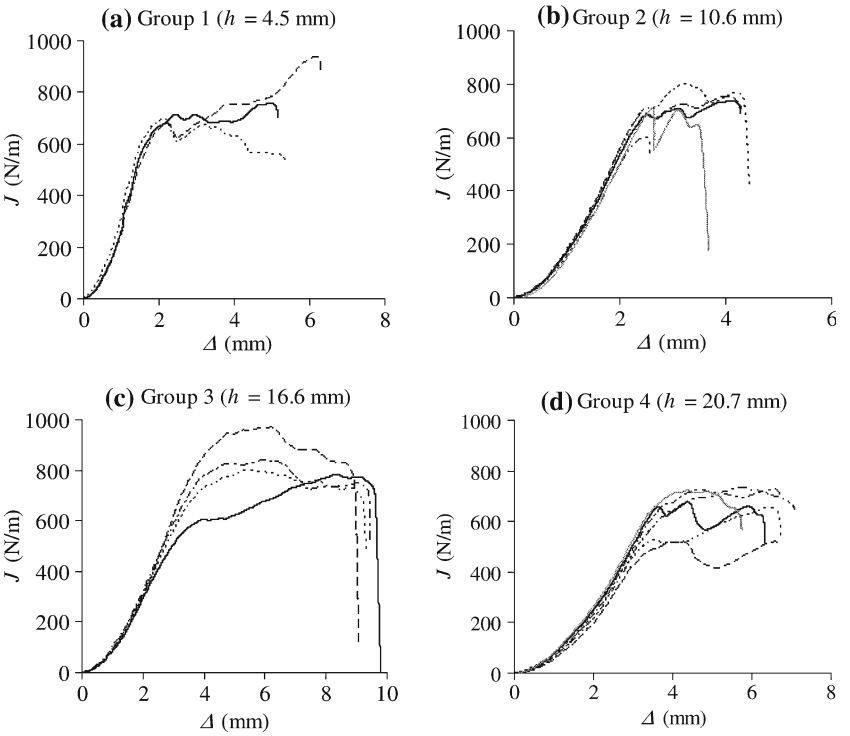

Fig. 12 Experimental $J(\Delta)$ curves

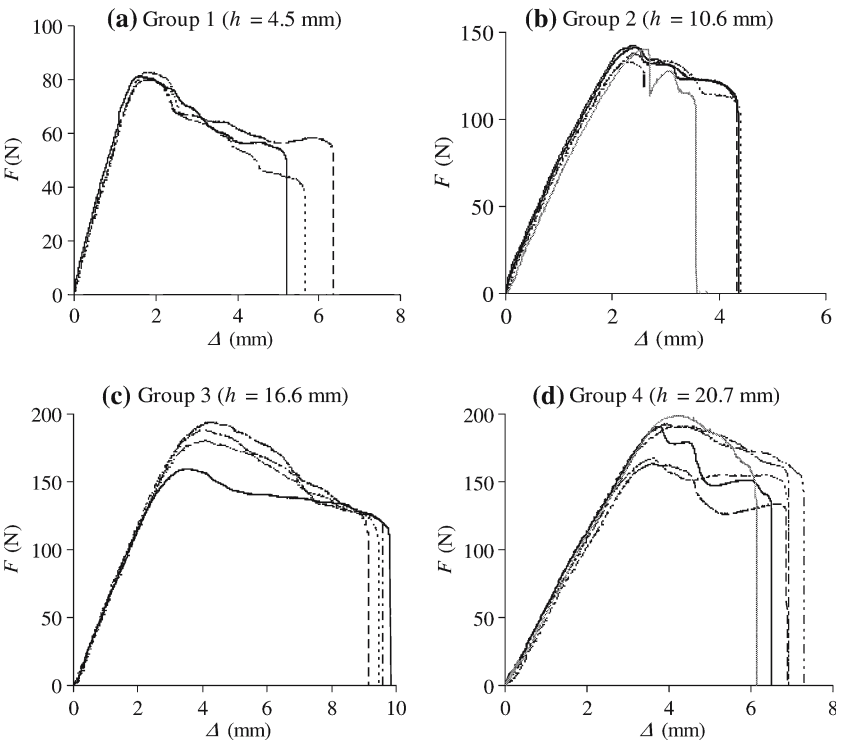

Fig. 13 Experimental $F(\Delta)$ curves

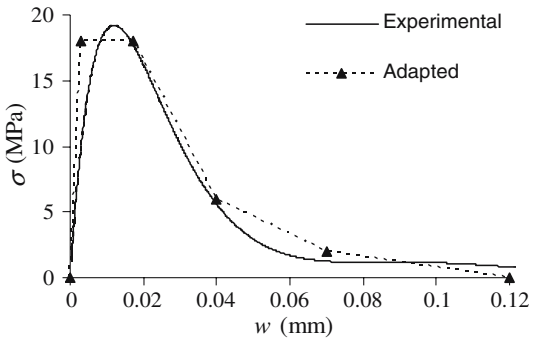

Fig. 14 $\sigma(w)$ relations from an experiment and an approximation used in the simulations

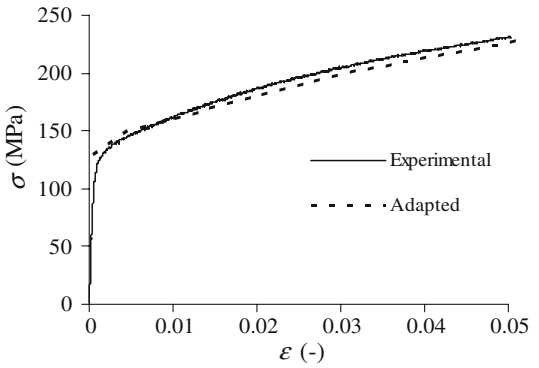

Fig. 15 Experimental $\sigma(\varepsilon)$ relation of the adherends and an approximation used in the simulations

curve, (Fig. 14). The fracture energy is set to $J_c = 730\,\mathrm{J/m^2}$, which is consistent with the experimental results obtained in Section 4.1.

In order to achieve large plastic deformations of the adherends, mild steel with $\sigma_Y = 130\,\mathrm{MPa}$ is chosen. The true stress–strain curve for a uniaxial experiment is shown in Fig. 14 and it is assumed to be well described by an isotropic elastic-plastic material model with non-linear hardening shown in Fig. 15. The non-linear part of the curve is built up by piecewise linear hardening parts. With this model, the adherends are expected to deform plastically before the adhesive looses its load bearing capacity.

With the behaviour of the adherends and the adhesive layer determined as described, simulations are used to determine an appropriate specimen design. The final design of Group 5 is given in Table 2.

With this choice, the length of the damage zone, d_s, is expected to be roughly 3 mm, which can be compared with the minimum length, $\sim 7\,\mathrm{mm}$, with the elastic adherends. Moreover, the specimens deform plastically before the adhesive reaches the critical deformation, w_c. At w_c the largest plastic strain and the length of the plastic zone in the adherends are approximately 1.5% and 12 mm, respectively.

A total number of eight specimens are manufactured. These are manufactured in the same way as described in Section 3.3.

5.2 Experimental and numerical results

The experiments confirm that the adherends deform plastically before any macroscopic crack becomes visible. However, visual inspections of the adherends reveal that the adherends deform with a considerable amount of anticlastic bending. In order to investigate if this effect influences the results a shell model is developed in ABAQUS.

In the analysis we consider large deformations and one symmetry plane is utilized, therefore only one of the adherends is modelled. The adherend is modelled with shell elements (S4) and the adhesive layer with the same spring elements (SPRING1) as in the beam model described in Section 3.3. The force–displacement relation for the spring element is given by the model described in Fig. 14.

For the spring elements that are located at the interior nodes of the adhesive layer, the force is calculated by $F = \sigma(w)\, b_e l_e$, where $b_e = 0.2\,\mathrm{mm}$ is the width and $l_e = 0.4\,\mathrm{mm}$ is the length of the shell element, respectively. At the edges of the adhesive layer (except for the four corners) the force in the springs is $F/2$ and at the corners it is $F/4$. The model consists of 3,200 shell elements and 2,091 spring elements.

The result from the shell model is shown in Fig. 17 together with the experimental result. With the fracture toughness set to $730\,\mathrm{J/m^2}$, the simulation adapt well to the first part of the curve where the behaviour is mainly determined by the elastoplastic behaviour of the adherends. However, the maximum load is obtained at a considerably smaller displacement, $\Delta \approx 23\,\mathrm{mm}$ as compared to the experimental value $\Delta \approx 40\,\mathrm{mm}$. Thus, the

Table 2 Final design of plastically deforming specimen

	h (mm)	a (mm)	l (mm)	b (mm)	d_s (mm)
Group 5	2	70	170	8	3

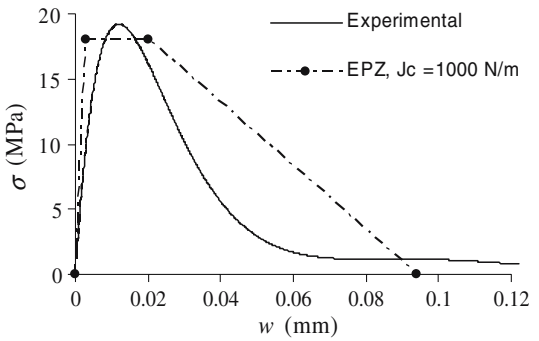

Fig. 16 Comparison between experiment and shell model for Group 5

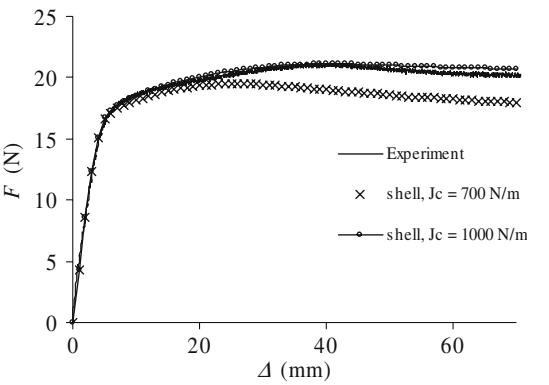

Fig. 17 Comparison between experiment and shell models for plastically deforming adherends

fracture toughness obtained from the elastic experiments is smaller than what is required to initiate fracture propagation in the experiments. This is in contrast to the results of Thouless et al. (1998) where a larger toughness is achieved with elastic adherends.

In a second simulation, the parameters of the EPZ model are changed to achieve an increased fracture energy, $J_c = 1,000\,\mathrm{J/m^2}$. The parameters are set to $w_1 = 3\,\mu\mathrm{m}$, $w_2 = 20\,\mu\mathrm{m}$, $\sigma_0 = 18\,\mathrm{MPa}$ and $w_c = 94\,\mu\mathrm{m}$, (Fig. 16). With these values, the simulated $F(\Delta)$ curve coincides with the experimental curve (Fig. 17).

The shell model is also capable of catching the apparent phenomenon of an increased strength, which a beam-element model fails to catch. Due to the anticlastic bending of the adherends, and the large deformations in these experiments, the strength of the adherends apparently increases since the cross section is higher. That is, the distance between the lower and upper edge of the cross section increases. This gives a higher sectional modulus. An interesting observation can be made from the simulation with the shell model; if the EPZ model is changed by choosing a higher value on σ_0 and a smaller value on w_c but maintaining $J_c = 1,000\,\mathrm{J/m^2}$, the loading at initial yielding decreases since the increased strength of the adhesive layer prevents the adherends from deforming anticlastically.

In the shell model, the crack starts to develop in the middle region at the start of the adhesive layer. This is due to the anticlastic bending which tends to increase the elongation of the adhesive layer in the middle region, (Fig. 18). For the model with $J_c = 1,000\,\mathrm{J/m^2}$, the crack starts to grow when $\Delta = 24\,\mathrm{mm}$. Thus, as shown in Fig. 17, the crack starts to develop in the layer before the maximum load is attained.

6 Length of the damage zone

In order to validate the adhesive layer theory we compare the structural behaviour obtained from simulations with experimental results. In Andersson and Stigh (2004), we compared the $F(\Delta)$ curves. Here, we make an attempt to extend the validation by also comparing the length of the damage zone. As indicated above, the adhesive is stress-whitening and this property is here used to indicate the length of the damage zone. In the experiments it is only possible to make an estimate of this length.

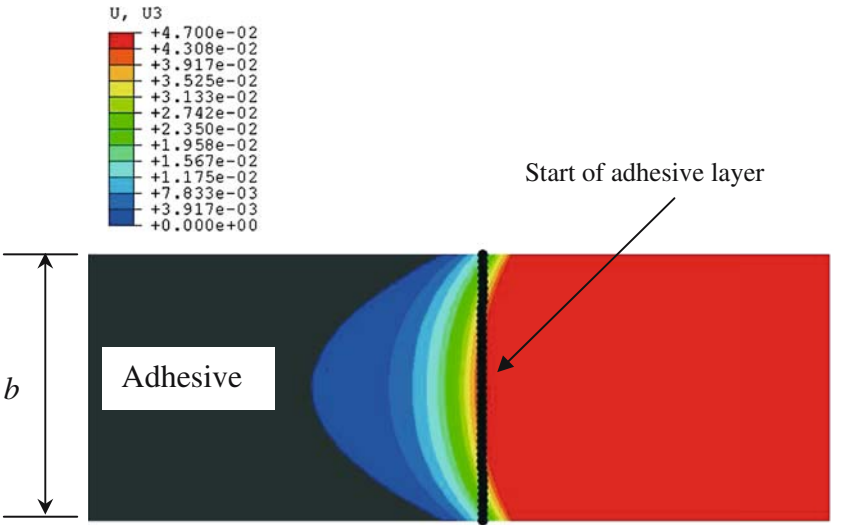

Fig. 18 Adhesive layer observed from above. Contour plot of the elongation, w, at $\Delta = 24$ mm for the shell simulation. U3 $= w/2$

The measurement of the length of the damage zone is made for two of the specimens from Group 2 ($h = 10.6$ mm) and two from Group 5 ($h = 2$ mm).

6.1 Elastically deforming adherends, Group 2

At these experiments, the tensile test machine is stopped at a specific value of the elongation, w, and the displacement, Δ is kept at a constant value. During the stop, photos are taken of the adhesive layer by means of the microscope. The microscope is gradually repositioned along the adhesive layer to capture about 5 mm of the layer at a time. This procedure takes about 15 min. A micrograph of the entire layer is build up afterwards by placing the photos side by side (Figs. 19 and 21). The lower part of each figure shows the light intensity, I_n, along the adhesive layer, for example, Fig. 19a. The light intensity is measured in a rectangular box with $12,900 \times 20$ pixels corresponding to a size of 40×0.06 mm. In order to smooth out disturbances in the layer, averaging is first performed in the vertical direction. A second averaging is performed in the horizontal direction where the intensity in a point is determined by taking the average of the intensity of 250 pixels on each side of the point of interest. As shown in a typical graph, for example, Fig. 19a, I_n varies considerably with x. To determine the length of the damage zone the following method is utilized: first, we fit a linear curve to the descending part of the intensity curve (Fig. 19a). Second, we fit a constant curve to the nearly constant part of the intensity curve. For the experiment of Fig. 19a, the adjustment is performed between $17.1 < x < 27.5$ mm and $27.9 < x < 36.6$ mm for the linear and constant parts, respectively. For the experiment of Fig. 19b, the adjustment is made between $17.9 < x < 29.3$ mm and $29.3 < x < 38.4$ mm for the linear and constant parts, respectively. Third, we take the intersection between descending linear curve and the constant curve as the endpoint of the damage zone. This point is thus taken as an estimate of the far end of the damage zone.

One of the experiments, (a) of Group 2 is stopped at $w = 110\,\mu$m and the other, (b) at $w = 85\,\mu$m. The critical elongation is roughly $80\,\mu$m for the experiments in Group 2 (Fig. 8b). Thus, for experiment (a), the macroscopic crack has propagated about 4 mm into the adhesive layer. Therefore, we chose to measure the length of the damage zone from this point. The light intensity along the layer is used to estimate the length of the damage zone $d_e \approx 24$ mm (where subscript e indicates experiment). Simulations with a $\sigma(w)$ relation according to the experimental curves of Group 2 (Fig. 20) gives $d_s \approx 18$ mm, which differs considerably from the experimental values. Thus, the experimentally estimated values of, d_e, is larger than the length determined from the simulations. However, if we make use of a typical experimental $\sigma(w)$ relation,

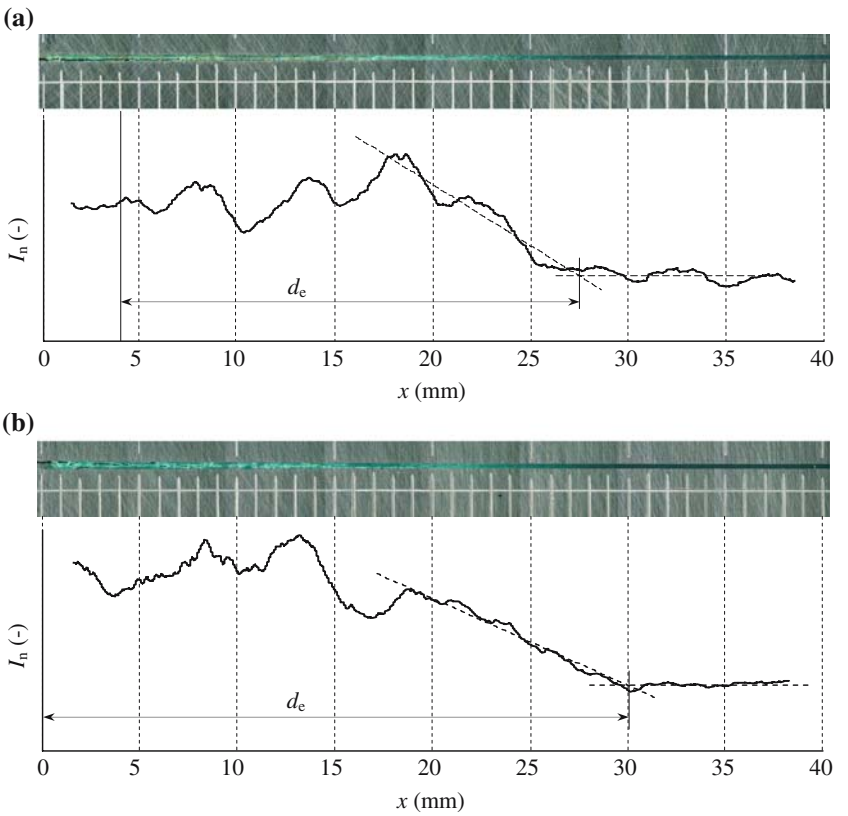

Fig. 19 Stress-whitening along the adhesive layer. Photos taken from two specimens in Group 2 ($h = 10.6$ mm). (**a**) At $w = 110\,\mu$m; (**b**) At $w = 85\,\mu$m. Distance between the vertical white lines in the lower adherend (below the adhesive) layer is 1 mm

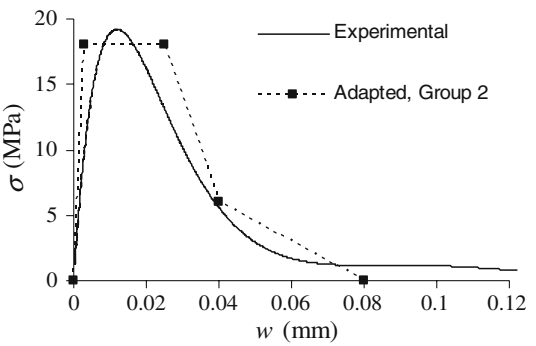

Fig. 20 $\sigma(w)$ relation used in the simulations to determine the length of the damage zone

as shown in Fig. 14, the damage zone becomes $d_s \approx 22$ mm, which is in tolerably good agreement with the experiments. For experiment (b), the length of the damage zone is $d_e \approx 30$ mm.

It is noted that the simulation using the $\sigma(w)$ relation according to a typical experimental curve gives $d_s \approx 22$ mm. By comparing this value with $d_e \approx 18$ mm, as is obtained with an experimental curve of Group 2, using the same values of J_c and σ_0 but with a different shape of the $\sigma(w)$ relation, we conclude that the length of the damage zone is very sensitive to the shape of the $\sigma(w)$ relation and especially to the descending part of the relation.

A disadvantage with the present method is that the elongation w increases and the applied force decreases when Δ is kept constant. Thus, the adhesive relaxes. This leads to a slight enhancement of the damage zone between each photo. However, this extension of the damage zone is estimated to be not more than a few millimetres and the photos should still provide a reasonable estimate of the damage zone length.

6.2 Plastically deforming adherends

A slightly different approach is used for the experiments with plastically deforming adherends. In these experiments it is not possible to measure the elongation w with the present experimental set-up since the specimen moves considerably due to

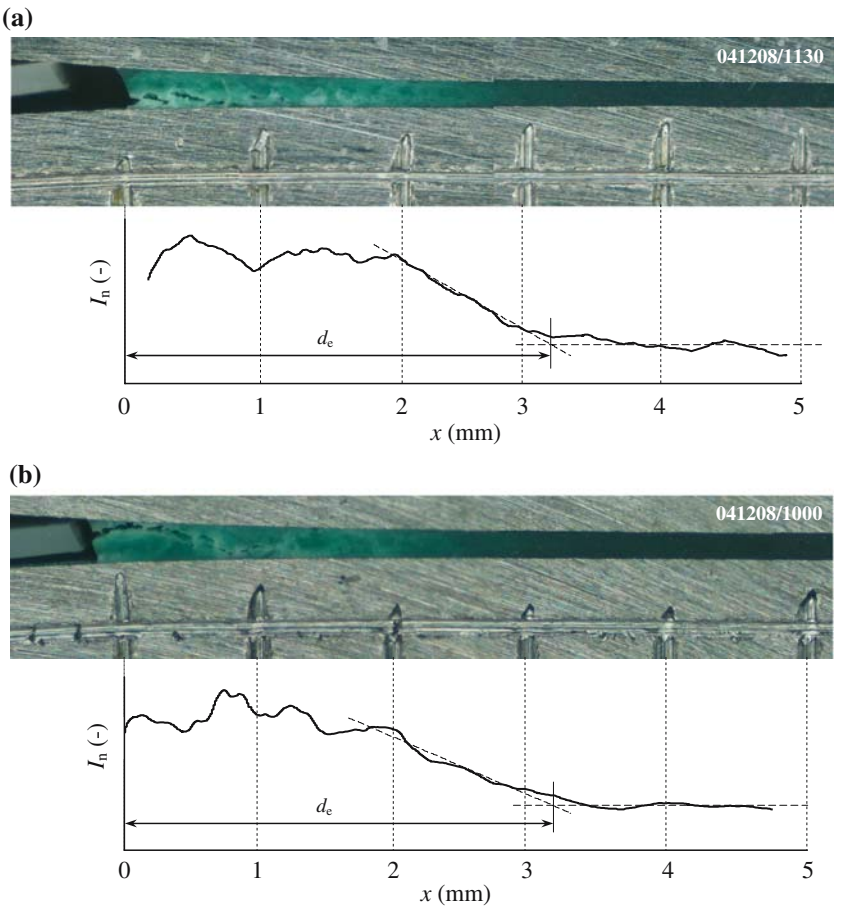

Fig. 21 Deformation of the adhesive layer. Images from Group 5 ($h = 2$ mm) near $F = F_{\max}$. Distance between the *vertical white lines* (below the adhesive) layer is 1 mm

the large deformations. Instead the tensile test machine is stopped when the force F reaches its maximum value and crack propagation is imminent. At this moment, Δ is kept constant and photos are taken. The entire damage zone is much smaller in these experiments and the entire length is captured with only two photos. In these experiments we do not encounter the problem with the relaxation of the adhesive when the tensile test machine is stopped.

The adhesive layer from the two experiments of Group 5 is shown in Fig. 21. The length of the damage zone is determined with the same method as before. In the same way as in Fig. 19, the lower part of each figure shows the light intensity, I_n, along the adhesive layer, for example, Fig. 21a. The light intensity is measured in a rectangular box with $4,200 \times 90$ pixels corresponding to a size of about 55×0.12 mm For the experiment of Fig. 20a, the adjustment is between $1.9 < x < 3.2$ mm and $3.2 < x < 4.9$ mm for the linear and constant part, respectively. For the experiment of Fig. 20b, the adjustment is between $1.8 < x < 3.1$ mm and $3.1 < x < 4.9$ mm for the linear and constant part, respectively. The averaging in the horizontal direction is determined by taking the average of the intensity of 200 pixels on each side of the point of interest. In these experiments, the length of the damage zone is estimated to about 3.1 mm for both the experiments. Thus, $d_e \approx 3.1$ mm.

To compare the result with simulations, we apply the shell model with $J_c = 1,000$ J/m^2 using the EPZ model shown in Fig. 16. The length of the damage zone is measured at the same place as in the experiments, that is, along one side of the specimen. With this model the length of the damage zone is roughly 2 mm. Thus, the experimentaly determined d_e is larger than the one obtained from the simulation. It should be observed that the EPZ model only gives an estimate of the length of the damage zone.

As noted in the previous subsection, a model with a longer descending part would provide a better agreement with the experimental results. However, since the shape of the $\sigma(w)$ relation is unknown for these experiments we do not extend the analysis further.

In summary, for both Groups 2 and 5 the simulated lengths of damage zone are in reasonably good agreement with the experiments.

7 Conclusions and discussion

In this work we have investigated if the stress-elongation relation in peel ($\sigma(w)$) can be considered as a property associated with the adhesive layer. Experiments have been performed on the DCB specimen. Five different geometries have been tested. Four of these geometries are designed in such a way that the adherends deform elastically and with a damage zone, in the adhesive layer, considerably larger than the height of the adherends. In this case LEFM is not always applicable. From the experiments, a unique $\sigma(w)$ relation is established even though the length of the damage zone varies. The fracture energy and the maximum stress are found to be roughly 700 J/m^2 and 20 MPa, respectively. These results are consistent with the results of Andersson and Stigh (2004). In addition, we also compare the length of the damage zone obtained from the experiments with numerical simulations. These are found to be in reasonably good agreement which further supports the method. It is also established that the length of the damage zone is very sensitive to the shape of the $\sigma(w)$ relation and especially to the descending part.

When the $\sigma(w)$ relation obtained from the elastic experiments is used to simulate experiments where the adherends deform plastically the simulations fail to predict the outcome of the experiments. It is necessary to increase the fracture energy to about 1,000 J/m^2 in order to achieve good agreement with the experiments. This result indicates that the adhesive layer theory and consequently the stress-elongation relation have limited applicability. The limit of applicability is an important topic for future research.

The difference between the fracture toughness obtained from the two types of experiments may depend on several factors. It is noted that, for the experiments where the adherends deform plastically, a higher level of in-plane strain is induced in the adhesive layer. This is due to the significant amount of plastic strain occurring in the adherends near the start of the adhesive layer. For Group 5 ($h = 2$ mm) the strain in the adherends attains $\varepsilon = 1.5\%$ at the adhesive layer. As a consequence the hydrostatic stress in the layer increases. If plasticity of the adhesive layer is responsible for the increased toughness, it would require a larger force to initiate plasticity in the adhesive layer in this case. However, it is not likely that plasticity is the toughening mechanism. In Andersson and Stigh (2004) it is concluded that the damage process starts before any major amount of plasticity initiates. A study that supports this conclusion is made by Chen and Dillard (2001), where DCB experiments with a superimposed T-stress acting parallel to the layer are performed. No difference in toughness is observed either with zero T-stress or with a considerable tensile T-stress.

As pointed out in Section 4.2, the fracture energy of the adhesive varies along the layer. This is attributed to different fracture processes along the layer; probably due to the inhomogeneous structure of the material. With the elastically deforming adherends, the damage zone is long; 4–10 times longer than in the experiments where plastic deformation occurs in the adherends, and the probability of finding a weak region within the damage zone is therefore considerably larger. In addition, the applied peel stress on the adhesive layer is nearly constant along a considerable part of the layer due to the high stiffness of the adherends. Therefore, a possible macroscopic crack is likely to start at the weakest point along the layer. These cracks can either propagate or be arrested depending on the material and loading in the vicinity of the weaker region. It is also noted that the adherends store a substantial amount of elastic energy in the experiments where the adherends deform elastically. This energy tends to be released. Thus, the adhesive layer is subjected to a prescribed force rather than to a prescribed displacement. As a consequence, when a weak region becomes unstable it looses its loading capacity and the loading capacity of the complete joint decreases. This may explain the variation of the J_c values in the experiments where

the adherends deform elastically (Fig. 9). In the experiments where the adherends deform plastically the stored elastic energy is almost negligible. Thus, in this case the adhesive is subjected to a condition of prescribed displacement, which renders this experiment more stable.

A plausible explanation for the variation of the fracture energy with the behaviour of the adherends is provided by Cavalli and Thouless (2001). They argue that the fracture toughness of an adhesive layer depends on the different levels of constraints imposed by the adherends. The constraint has the effect of triggering different types of deformations mechanisms which alters the stress state in the layer. However, for the present adhesive no such change in deformation mechanism is observed; no apparent difference in the appearance of the fracture surfaces can be observed between the experiments with the two types of deforming adherends.

The results stated here imply that the DCB specimen is not a completely stable specimen. In future work, this will be examined.

Acknowledgements The authors would like to thank Prof. Ulf Stigh for fruitful discussions during this work and for valuable suggestions regarding the manuscript. The authors would also like to thank Mr Stefan Zomborcsevics and Mr Eiler Karlsson for their help with the manufacturing of the test specimens.

References

Alfredsson KS, Biel A, Leffler K (2003) An experimental method to determine the complete stress-elongation relation for a structural adhesive layer loaded in shear. In: Proceedings of the 9th international conference on the mechanical behaviour of materials

Andersson T, Stigh U (2004) The stress-elongation relation for and adhesive layer loaded in peel using equilibrium of energetic forces. Int J Solids Struct 41:413–434

ASTM D3433 (1999) Fracture strength in cleavage of adhesive in bonded joints. American Society for Testing and Materials, Philadelphia, USA

Biel A (2005) Constitutive behaviour and fracture toughness of an adhesive layer. Thesis for the degree of licentiate in engineering, Chalmers University of Technology

British Standard, BS7991:2001 (2001) Determination of the mode I adhesive fracture energy G_{IC} of structure adhesives using the double cantilever beam (DCB) and tapered double cantilever beam (TDCB) specimens. British Standard Institution, London, Great Britain

Cavalli MN, Thouless MD (2001) The effect of damage nucleation on the toughness of an adhesive joint. J Adhesion 76:75–92

Chen B, Dillard DA (2001) The effect of T-stress on crack path selection in adhesively bonded joints. Int J Adhesion Adhesives 21:357–368

Eshelby JD (1951) The force on an elastic singularity. Philosophi Trans Royal Soc Lond Ser A 244:87–112

Högberg JL, Stigh U (2006) Specimen proposals for mixed-mode testing of adhesive layer. Eng Fracture Mech 73:2541–2556

Klarbring A (1991) Derivation of a model of adhesively bonded joints by the asymptotic expansion method. Int J Eng Sci 29:493–512

Leffler K, Alfredsson KS, Stigh U (2006) Shear behaviour of adhesive layers. To appear in Int J Solids Struct

Olsson P, Stigh U (1989) On the determination of the constitutive properties of thin interphase layers—an exact solution. Int J Frac 41:R71–R76

Rice JR (1968) A path independent integral and the approximate analysis of strain concentration by notches and cracks. J Appl Mech 33:379–385

Salomonsson K, Andersson T (2006) Modelling and parameter calibration of an adhesive layer at the meso level. Submitted for publication

Sørensen BF (2002) Cohesive law and notch sensitivity of adhesive joints. Acta Materialia 50:1053–1061

Stigh U (1988) Damage and crack growth analysis of the double cantilever beam specimen. Int J Fracture 37:R13–R18

Stigh U, Andersson T (2000) An experimental method to determine the stress-elongation relation for a structural adhesive loaded in peel. In: Williams JG, Pavan A (eds) Proceedings of the second ESIS conference on fracture of polymers, composites and adhesives. ESIS publication 27, Elsevier, pp297–306

Su C, Wei YJ, Anand L (2004) An elastic-plastic interface constitutive model: application to adhesive joints. Int J Plasticity 20:2063–2081

Thouless MD, Adams JL, Kafkalidis MS, Ward SM, Dickie RA, Westerbeek GL (1998) Determining the toughness of plastically deforming joints. J Materials Sci 33:189–197

Tvergaard V, Hutchinson JW (1992) The relation between crack growth resistance and fracture process parameters in elastic-plastic solids. J Mech Phys Solids 40:1377–1397

Yang QD, Thouless MD, Ward SM (1999) Numerical simulations of adhesively-bonded beams failing with extensive plastic deformation. J Mech Phys Solids 47:1337–1353